Prevention of autosomal dominant retinitis pigmentosa by systemic drug therapy targeting heat shock protein 90 (Hsp90)

Lawrence C. S. Tam*, Anna-Sophia Kiang, Matthew Campbell, James Keaney, G. Jane Farrar, Marian M. Humphries, Paul F. Kenna, and Pete Humphries

The Ocular Genetics Unit, Department of Genetics, Trinity College Dublin, Dublin 2, Ireland

*To whom correspondence should be addressed. Tel: +353 (0)18962484; Fax: +353 (0)18963848; Email: lawrenct@tcd.ie

Abstract

Retinitis pigmentosa (RP) is the most prevalent cause of registered visual handicap among working aged populations of developed countries. Up to 40% of autosomal dominant cases of disease are caused by mutations within the rhodopsin, RDS-peripherin and inosine 5'-monophosphate dehydrogenase type 1 (IMPDH1) genes, at least 30 mutations within which encode proteins that cause disease pathology by misfolding and aggregation. Given the genetic complexity of this disease, therapies that simultaneously target multiple mutations are of substantial logistic and economic significance. We show here, in a murine model of autosomal dominant RP (RP10) involving expression of an Arg224Pro mutation within the IMPDH1 gene, that treatment with the low molecular weight drug, 17-allylamino-17-demethoxygeldanamycin (17-AAG), an ansamycin antibiotic that binds to heat shock protein Hsp90, activating a heat shock response in mammalian cells, protects photoreceptors against degeneration induced by aggregating mutant IMPDH1 protein, systemic delivery of this low molecular weight drug to the retina being facilitated by RNAi-mediated modulation of the inner blood-retina barrier. 17-AAG has orphan drug status and is in current clinical use for treatment of non-neuronal diseases. These data show that a single low molecular weight drug has the potential to suppress a wide range of mutant proteins causing RP.

Introduction

Retinitis pigmentosa (RP), an hereditary degenerative retinopathy resulting in progressive loss of rod and cone photoreceptors, is generally regarded as the most significant cause of registered visual handicap in the developed world (1). At the genetic level, it is one of the most heterogeneous of inherited conditions, segregating in autosomal dominant, recessive or X-linked recessive modes, and approximately 40 genes having been implicated in disease pathology (RetNet; http://www.sph.uth.tmc.edu/RetNet). Symptomatically, RP is a highly variable disorder, where patients may develop visual loss in early childhood, while others may remain asymptomatic until mid-adulthood. In most cases, death of rod cells results in the development of night blindness with visual field restrictions, and subsequent loss of cone cells may lead to complete loss of visual fields. In terms of therapeutic intervention, progress is being made in validation both of gene replacement therapies and in RNAi-mediated suppression of transcripts encoding dominantly mutated proteins (2-6). Autosomal dominant forms of RP represent up to 30% of all cases, and within this category, approximately 40% of cases are caused by mutations within the rhodopsin, inosine 5'-monophosphate dehydrogenase type 1 (IMPDH1) and RDS-peripherin genes (7-10). To date, over 140 point mutations identified in the rhodopsin gene are known to cause autosomal dominant RP (adRP), and almost one sixth of those may be implicated in disease pathology through protein misfolding (11). In particular, extensive studies into the pathological mechanism of mutant P23H opsin, which is the most frequent mutation responsible for adRP in the North American population (accounting for ~25% of all rhodopsin mutations), has increased our understanding of the role that protein misfolding plays in photoreceptor cell death.

In brief, the P23H missense mutation renders rhodopsin extremely aggregation prone, leading to the recruitment of endoplasmic reticulum (ER)-resident chaperones (e.g. BiP and GRP94) and initiation of an auto-cellular control response termed the unfolded protein response (UPR) to disengage protein synthesis and favor protein degradation. Accumulation of misfolded opsin within the ER imposes serious cellular stress and ER-localised chaperones retro-translocate mutant opsins from the ER to the ubiquitin-proteasome system (UPS) for degradation in the cytosol (11-13). When the ubiquitin-proteasome system eventually becomes overloaded with mutant opsins, the buildup of toxicity may initiate a detrimental cascade leading to photoreceptor cell death through apoptosis (11, 12). Fewer studies have been undertaken to identify aggregation properties associated with mutations within the RDS-peripherin gene. However, some mutations have been implicated in protein misfolding, including the RDS missense mutation N244K (14). Previously, we reported that one of the missense mutation (Arg224Pro) in the IMPDH1 gene responsible for the RP10 form of adRP, identified in a large Spanish family, causes significant protein tertiary structural perturbation pushing the folding equilibrium towards intermediates that have a propensity to misfold and aggregate, resulting in the formation of insoluble protein aggregates in cell cytosol (9, 15). IMPDH1 is a rate limiting enzyme in the *de novo* biosynthesis pathway for guanine nucleotides and is highly expressed in rod outer segments (15). Enzymes of the nucleotide biosynthesis pathway are important in supporting normal cellular function and play crucial regulatory roles in the photo-transduction pathway. Recently, we reported that adeno-associated virus (AAV)-mediated expression of mutant human IMPDH1 bearing the Arg224Pro mutation in the RP10 mouse model impairs visual function and induces rapid photoreceptor cell death (3). Although the exact mechanism of

toxicity acquired by mutant IMPDH1 still remains to be elucidated, the pathological hallmarks displayed in the RP10 mouse model suggest that it is likely to be a dominant negative effect similar to that observed in the P23H mutant rhodopsin mouse model (16). Taken together, these data open up a potential avenue of common therapy for multiple forms of adRP, based on suppression of protein aggregation.

Mammalian cells are equipped with an intricate surveillance network that assists in the folding of a polypeptide chain to its functionally competent three-dimensional structure. Molecular chaperones are a set of conserved endogenous cellular regulators of protein conformational change and are also part of the defense mechanism against different kinds of cellular stress. Their main tasks involve normal folding of nascent polypeptides by binding to hydrophobic regions, and to prevent abnormal interactions between non-native proteins, enhance *de novo* protein folding, and promote refolding or directing misfolded proteins for proteasome degradation (17). Hence, genetic dysfunctions of chaperones have been associated with a range of diseases such as dilated cardiomyopathy (a non-ischemic cardiomyopathy associated with mitochondrial heat shock protein 40 deficit, Williams syndrome (a rare neurodevelopmental disorder caused by deletion of numerous genes, including genes encoding heat shock protein 27) and Leber congenital amaurosis (LCA) (retinal dysfunction associated with mutations in the aryl hydrocarbon receptor interacting protein like 1 gene, AIPL1) (18-21). Chaperoning is carried out by a distinct group of cellular proteins originally known as heat shock proteins which are particularly abundant in cells subjected to environmental stress (22). To date, more than 20 different chaperone families have been identified, with each providing different structural support to maintain protein homeostasis. Heat shock protein 90 (Hsp90; 90-kDa)

is one of the most abundant molecular chaperones in eukaryotic cells that resides

in the cytosol comprising 1-2% of total cellular proteins under normal conditions

(23). Mammalian cells possess three major forms of Hsp90 proteins located in the

cytoplasm (Hsp90-α and Hsp90-β), mitochondria (TRAP-1) and ER (GRP94).

The existence of Hsp90 in different cellular compartments illustrates that it is a

global cellular regulator central to the folding, activation and assembly of a wide

array of cellular proteins, known as 'client' proteins. To date, there are over 100

identified Hsp90 client proteins, including transcription factors (e.g. hypoxia-

inducible factor-1α, HIF-1α) and tyrosine kinases (e.g. ErbB2, CDK-4)

(http://www.picard.ch/downloads/Hsp90interactors). The dependence of these

client proteins on Hsp90 for stability and activity shows the importance of this

chaperone in essential housekeeping functions such as cellular trafficking,

chromatin remodeling, cell growth, signal transduction and differentiation.

Among other cytosolic chaperones, the 70-kDa heat shock protein (Hsp70)

chaperone is one of the best-documented and mechanistically understood (24). In

eukaryotes, cytosolic Hsp70 and Hsp90 chaperones function intimately with a

series of co-chaperones to assist in the folding of newly synthesised polypeptides

and target damaged proteins for ubiquitin-mediated proteasome degradation (Fig.

1) (23, 25). The cellular chaperone machinery is adept at correctly folding large

quantities of protein, however when this system is overwhelmed with protein in

its non-native conformation (caused by one of many adverse conditions such as

destabilizing mutations), one of a diverse range of protein-folding diseases may

ensue. The consequences of aberrant protein can manifest in two ways (Fig. 1);

(a) the function of an enzyme is lost as a result of the protein's inability at

attaining a functional conformation, and thus resulting in clearance via

proteasome degradation with a consequent 'loss of function' phenotype (e.g.

MKKS/BBS6 in Bardet-Biedl Syndrome) (26); (b) in contrast, an accumulation of misfolded protein result in aggregation or the formation of insoluble proteinasceous deposits that adversely affect cell function and cause a 'gain of function' toxicity (e.g. P23H mutation in rhodopsin) (11).

Manipulation of the cellular chaperone machinery either by over-expression of exogenous chaperones or the use of pharmacological chaperone inducers have been evaluated in many model systems to counteract protein misfolding by enhancing the endogenous folding capacity (27, 28). Since Hsp70 is induced during normal cellular stress response and is involved in the folding of a wide variety of proteins, therapeutic elevation of this chaperone has been considered to be an attractive strategy for the treatment of many disorders arising from protein misfolding. The augmentation of Hsp70 has demonstrated beneficial effects in many over-expression studies of different disease models. For example, co-expression of Hsp70 and Hsp40 in a *Drosophila* model of poly-glutamine disease has been reported to synergistically suppress misfolding and cytotoxicity of the poly-glutamine protein (28, 29). Recently, AAV-mediated over-expression of an ER homologue of Hsp70 (BiP/Grp78) significantly reduced photoreceptor cell death and maintained visual function in the transgenic P23H rhodopsin rat model (30). Currently, many low molecular weight pharmaceutical agents have demonstrated the ability to increase cellular expression of Hsp70 through the inhibition of Hsp90 (31). Pharmacological up-regulation of Hsp70 expression is one of the most validated methods of inducing cellular chaperones via intervention of the heat shock factor-1 (HSF-1) pathway as shown in Fig. 2. The inability of cells to efficiently increase levels of Hsp70 by this mechanism may be responsible for the underlying cause of gradual accumulation of pathological mutant protein aggregates. Therefore it is of no surprise that most

neurodegenerative diseases manifest in late adulthood, when chaperone

inducibility and activity are compromised with ageing and disease (32). One of the

first classes of Hsp90 inhibitors, geldanamycin (GA), was initially designed to be

used as an anti-tumor drug based on its ability to induce client protein degradation

that included a wide variety of proto-oncogenic protein kinases and nuclear

hormone receptors (33). Subsequently, Zou and colleagues also showed that GA

has the ability to disrupt and breakdown the Hsp70/Hsp90/HSF-1 complex,

triggering the activation of heat shock response in mammalian cells (34).

However, GA is highly hepatotoxic and displays unfavorable pharmacokinetic

properties and solubility rendering it to be unsuitable for clinical use. A semi-

derivative of GA, 17-allylamino-17demethoxygeldanamycin (17-AAG, molecular

weight: 585.69), has been shown to elicit significantly improved toxicity profile

and bioavailability compared to GA (35, 36). Most importantly, it has displayed

excellent efficacy in combating protein aggregation in model systems of

polyglutamine-induced neurodegeneration and spinal and bulbar muscular atrophy

(SBMA) (37, 38). Recently, Mendes and colleagues also illustrated that

administration of 17-AAG in mammalian cells enhanced P23H folding and

reduced the dominant negative effect on wild type (WT) opsin processing, as well

as reducing toxic gains-of-function effect (39).

 Using a murine model of the RP10 form of adRP, we show here that

administration of 17-AAG intra-vitreally results in highly effective reduction of

mutant IMPDH1 aggregation and protection of the outer nuclear layer (ONL)

structure. In addition, RNA interference (RNAi)-mediated reversible modulation

of the inner blood retina barrier (iBRB) enables systemic administration of 17-

AAG at low, periodic doses to achieve therapeutic effects in the RP10 mouse

model. 17-AAG has orphan drug status for the treatment of chronic myeloid

leukemia (Bristol-Myers Squibb International Corporation), and is already in clinical use in the treatment of a number of non-neuronal conditions (40). These results indicate that a common systemic drug therapy could be used in the treatment of up to 30 genetically distinct forms of adRP.

Results

Expression of human mutant IMPDH1 in HeLa cells induces the formation of insoluble protein aggregates and cell death

The correlation of protein aggregation with the development of many debilitating human conformational disorders has stimulated the development of several computer prediction models to anticipate the aggregation propensities of potentially pathological polypeptides. Therefore, we employed two computer-based folding algorithms to briefly examine how two disease causing RP10 mutations, Arg224Pro and Asp226Asn (9, 10), might affect the folding capacity of human IMPDH1 protein. First, the IMPDH1 peptide sequence (Protein Data Bank accession number: 1JCN) was submitted to 'Aggrescan', which is a web-based software used for the prediction of aggregation-prone segments in protein sequences (41). Aggrescan analysis showed that human IMPDH1 sequence contains 21 'hotspot areas', which denote aggregation-prone segments in a given protein sequence. Moreover, the amino acid at position 224, at which the missense mutation of interest occurs, was predicted to lie within an aggregation-prone segment, whereas the amino acid at position 226 was not identified in such a segment. This suggested that changes at amino acid 224 may have a higher propensity to perturb protein structure and induce protein aggregation

(Supplementary data, Fig. S1). In addition, computer modelling algorithm, PopMuSic-2.0, was used to predict thermodynamic protein stability changes upon point mutations in human IMPDH1 (42). Interestingly, computer analysis predicted that a change at amino acid 224 from arginine to proline in human IMPDH1 yielded a higher folding free energy change ($\Delta\Delta G$ = 1.44 kcal/mol) than that observed from a change of aspartic acid to asparagine at position 226 ($\Delta\Delta G$ = -0.06 kcal/mol). This finding suggested that the former mutation may have a more destabilizing folding effect on human IMPDH1 protein structure than the latter.

Previous data obtained in our laboratory had shown that expression of mutant IMPDH1 bearing the Arg224Pro mutation in HEK 293T cells exhibited considerable decreased protein solubility, whereas expression of both WT IMPDH1 and mutant IMPDH1 bearing the Asp226Asn mutation showed no decrease in protein solubility (15). Therefore, we repeated this experiment again using antibody detection of WT and mutant IMPDH1 proteins rather than His-tag protein that was reported in the previous study (15). Similar to previous findings, we carried out a cellular fractionation assay where proteins were separated into whole cell lysates, soluble cytosolic fraction, nuclear and insoluble pellet fraction, which were subsequently analysed by SDS-PAGE electrophoresis. Both WT and mutant IMPDH1 proteins were expressed in whole cell lysates, whereas only WT IMPDH1 protein was found in the soluble cytosolic fraction and mutant IMPDH1 (Arg224Pro) mainly localised in the insoluble protein pellet fraction (Supplementary data, Fig. S2). In order to examine whether the formation of insoluble protein aggregates was a concentration-dependent effect *in vitro*, a titration study was carried out whereby a range of human WT and mutant IMPDH1 expression plasmids (250 ng to 1 ng) were transfected into 5 x 10^5 HeLa

cells which were then harvested 48 hours later by cellular fractionation. In the insoluble pellet fraction, IMPDH1 at 55 kDa was detected in HeLa cells transfected with 250 ng and 50 ng of Arg224Pro mutant IMPDH1, whereas no IMPDH1 protein was detected in cells transfected with either empty vectors or WT IMPDH1 throughout the different concentration range of expression plasmids (Fig. 3A). A weak IMPDH1 band at 55kDa was only detected in the insoluble fraction from cells transfected with 250 ng mutant IMPDH1 bearing the Asp226Asn mutation (Fig. 3A), which may suggest that this particular mutation may have a low propensity to cause folding disruption, but the effect was not as profound as those seen in the Arg224Pro mutation. Hence, these data provide further evidence that mutant IMPDH1 bearing the Arg224Pro mutation forms insoluble aggregates in a dose-dependent manner in mammalian cells (Fig. 3A).

In order to examine whether over-expression of WT and mutant IMPDH1 in HeLa cells would induce significant cell death *in vitro*, HeLa cells were transfected either with 1 μg of WT or mutant IMPDH1 EGFP fusion plasmids, and an empty EGFP vector was also included to account for cell death induced by transfection agents. Twenty-four hours post-transfection, HeLa cells were fixed and stained with cleaved caspase-3 antibody as shown in Fig. 3B. Caspase-3 is one of the key executioners of apoptosis, as it is responsible for the proteolytic cleavage of many key proteins such as the nuclear enzyme poly ADP-ribose polymerase (PARP) (43). Activation of caspase-3 requires proteolytic processing of its inactive zymogen into activated p17 and p12 fragments and cleavage of caspase-3 requires aspartic acid at the P1 position (44). The cleaved caspase-3 antibody detects endogenous levels of the large fragment of activated caspase-3 resulting from the cleavage adjacent to Asp175. The quantification of positive cleaved caspase-3 stained cells measured against transfection efficiency showed that the expression

of human mutant IMPDH1 (Arg224Pro) in mammalian cells induced a

significantly higher level of cell death (40.44 ± 5.99%) than WT IMPDH1 (11 ±

2.25%; $P < 0.001$) or empty control vectors (3.74 ± 0.73%; $P < 0.001$) (n=3) (Fig.

3B). In addition, cell blebbing, a term used to describe dissociation of the cell's

cytoskeleton during apoptosis, was also predominantly observed in HeLa cells

transfected with mutant IMPDH1 as shown in Fig. 3C. Immunoprecipitation

analysis also showed that mutant IMPDH1 associates with both Hsp70 and Hsp90

in HeLa cells as shown in Fig. 3D, suggesting that molecular chaperones may be

recruited to the misfolded protein to prevent aggregation by correcting the folding

defect or target them for proteasome degradation. Collectively, these data provide

evidence that the expression of human mutant IMPDH1 bearing the Arg224Pro

mutation forms insoluble protein aggregates, which causes an elevated level of

apoptosis in mammalian cells.

17-AAG mediated induction of heat shock response in HeLa cells and

suppression of insoluble mutant IMPDH1 protein aggregates

In order to investigate whether inhibition of Hsp90 will induce a heat shock

response in mammalian cells, HeLa cells were treated with 17-AAG (2 μg per 1 x

10^5 cells) or DMSO (0.02 %) and total RNA was extracted at four different time

points post-treatment (6, 24, 48 and 72 hours). Transcript levels of Hsp40, Hsp70

and Hsp90 were quantified by Real-Time RT-PCR using specific primers and

normalised against endogenous house-keeping β-actin gene expression. RT-PCR

data showed that all heat shock protein transcripts increased gradually over time

following 17-AAG treatment (Fig. 4A). Similarly, induction of heat shock protein

expression was examined forty-eight hours post-treatment with 17-AAG (10 μg

per 5 x 10^5 cells) or DMSO (0.05 %) in HeLa cells by Western blot analysis using

specific antibodies. As shown in Fig. 4B, expression of Hsp70 was significantly increased after treatment with 17-AAG as compared to DMSO control (2.39 ± 0.18 fold increase; $P = 0.024$), whereas Hsp90 and Hsp40 were only mildly increased (1.69 ± 0.15; $P = 0.095$ and 1.42 ± 0.11; $P = 0.19$, respectively). In order to determine whether induction of heat shock proteins by 17-AAG treatment would have an effect on insoluble mutant IMPDH1 protein aggregates, HeLa cells were first transfected with a mutant IMPDH1 expression plasmid bearing the Arg224Pro mutation (0.5 µg per 5 x 10^5 cells), and subsequently treated with 17-AAG (10 µg per 5 x 10^5 cells) or DMSO (0.05%) as control 4-6 hours post-transfection. Forty-eight hours post-treatment, HeLa cells were lysed and analysed by cellular fractionation assay for the presence of insoluble mutant IMPDH1 protein aggregates. Using this assay, insoluble mutant IMPDH1 protein can be immunologically detected in cells treated with DMSO control in the insoluble pellet fraction (Fig. 4C). In contrast, treatment of HeLa cells with 17-AAG significantly reduced insoluble mutant IMPDH1 protein aggregate levels to $43 \pm 3.98\%$ in the pellet fraction as compared to control ($P = 0.0011$; n=3) (Fig. 4C). The levels of mutant IMPDH1 protein in whole cell lysates were also found to be reduced following 17-AAG treatment as compared to controls (Supplementary data, Fig. S3), suggesting that the induction of heat shock proteins may favor the degradation of mutant IMPDH1 aggregates. Furthermore, reduction of insoluble mutant IMPDH1 protein aggregates by 17-AAG was accompanied with a decrease in the level of cleaved-caspase 3 activation as shown in Fig. 4D, indicating that 17-AAG is a potent inhibitor of mutant IMPDH1-induced apoptosis.

Rescue of photoreceptor cells in the RP10 mouse model by intra-vitreal delivery of 17-AAG

Previously, we described the rapid generation of a mouse model for RP10 by sub-retinal injection of AAV-2/5 expressing human mutant IMPDH1 bearing the Arg224Pro mutation in both heterozygous IMPDH1 and WT mice, whereby significant degeneration of the ONL was observed in both strains of animals four weeks post-AAV transduction (3). Therefore in this study, we employed the same strategy to generate the RP10 disease pathology in WT mice to evaluate the therapeutic effects of 17-AAG in targeting the cytoxicity associated with mutant IMPDH1 protein. First, we examined whether administration of 17-AAG *in vivo* will provoke a heat shock response similar to that observed in the initial *in vitro* study. Adult WT mice were intra-vitreally injected with 3 µl (0.2 µg/µl) of 17-AAG in the right eyes, and identical volumes of DMSO (2%) (vehicle control) were injected into the left eyes of these animals. 24 hours post-injection, retinas were lysed and the protein levels of Hsp40, Hsp70 and Hsp90 were determined by Western blotting. Densitometric analyses showed that relative amounts of Hsp70 were increased significantly as compared to DMSO controls (1.79 ± 0.13 fold increase; $P = 0.032$), and only marginal but non-significant up-regulations were observed in Hsp40 (1.49 ± 0.19 fold increase; $P = 0.16$) and Hsp90 (1.14 ± 0.07 fold increase; $P = 0.2$) (Fig. 5A). Induction of heat shock proteins by 17-AAG was also examined at further time points (48 and 72 hours) post intra-vitreal injection, and no major differences were observed between treated and control eyes (data not shown). This observation is in agreement with another report showing that robust induction of heat shock proteins in brain tissues was achieved at 24 hours post-treatment (45). To examine whether inhibition of Hsp90 is of therapeutic benefits in the RP10 mouse model, WT mice were first injected sub-

retinally with 3μl (1.4 x 10^{12} vp/ml) of rAAV-2/5 expressing human mutant IMPDH1 bearing the Arg224Pro mutation in both eyes to induce photoreceptor degeneration. Two weeks following the initial AAV injection, 3μl (0.2 μg/μl) of 17-AAG was intra-vitreally injected into the right eyes of these mice, and the same volume of DMSO (2%) was administered into the left eyes. An identical dose of 17-AAG or DMSO vehicle control was administered again on the fourth week after the initial AAV injection to sustain and maximise the potency of the inhibitor. On the fifth week after the initial AAV injection, all animals were sacrificed and eyes were extracted for both histopathological and Western blot analysis. As shown in Fig. 5B, the SDS-insoluble protein level of mutant IMPDH1 aggregates in the pellet fraction of eyes treated with 17-AAG (lanes 5 and 6) were significantly reduced to 18 ± 2.69 % as compared to DMSO controls (P = 0.0027; n=4) (lanes 3 and 4), whereas no insoluble mutant IMPDH1 aggregates were found in uninjected animals as negative controls (lanes 1 and 2). Furthermore, retinal sections from left eyes of mice injected with AAV-mutant IMPDH1 and subsequently treated with vehicle control showed significant deterioration in positively transduced ONL (Fig. 6A). In contrast, contralateral eyes treated with 17-AAG displayed substantially broader ONL in positively transduced areas (Fig. 6A). The average positively transduced ONL area per unit length between the left and right eyes was then compared, and eyes treated with 17-AAG displayed a significantly larger ONL area per unit length (29.45 ± 3.28 μm) than those treated with DMSO (18.63 ± 2.90 μm) (P = 0.0485; n=4) (Fig. 6B). These observations provide evidence that 17-AAG is able to protect photoreceptor cells form degeneration in the RP10 mouse model by inducing heat shock proteins to reduce the formation of mutant IMPDH1 aggregates.

Enhancement of 17-AAG systemic delivery to the inner retina by barrier modulation

While the results obtained above prove the principle of therapeutic strategy for treating the RP10 form of adRP by abrogating protein aggregation through intra-vitreal delivery of Hsp90 inhibitor, repeated drug administration would be required to maintain therapeutic efficacy. Moreover, repeated injection into the intra-vitreal space can lead to complications such as retinal detachment, haemhorrage and endophthalmitis. We therefore investigated the possibility of enhancing the efficiency of systemic delivery of 17-AAG to the retina using the recently described technique of barrier modulation (46). It has previously been shown in mice that RNAi-mediated down-regulation of transcripts encoding claudin-5, a protein component of the tight junctions comprising the blood-brain (BBB) and inner blood-retina barriers, results in the establishment of transient, reversible barrier permeability to very low molecular weight compounds of up to approximately 1 kDa (less than the molecular weight of two DNA base pairs), enough to allow passage from the peripheral circulation into the brain or retina of a wide range of low molecular weight drugs that can not normally gain access to these tissues, while excluding larger potentially damaging materials. According to the original experimental platform, claudin-5 siRNA is delivered systemically by high-pressure, high-volume tail vein injection, resulting in the induction of barrier permeability 24 hours post-siRNA inoculation, lasting for periods of up to 36 hours (47). We have found, however, that complexing siRNA with the polymer carrier, *invivoJetPEI*, siRNA can be introduced in low volume, allowing barrier modulation and hence systemic drug delivery on a periodic basis (46). Using this approach, WT mice were first sub-retinally injected with 3 µl of AAV-mutant224 (1×10^{12} vp/ml) in both eyes. Two weeks post-AAV transduction, 20 µg of

claudin-5 targeting or luciferase-targeting siRNAs coupled with the polymer *invivoJet-PEI*[(R)] were administered into mice by high pressure tail-vein injection to initiate transient modulation of the iBRB. Forty eight hours post-injection of siRNA, 17-AAG (30 mg/kg) was administered into all animals by intra-peritoneal injections. This time point was chosen on the basis of a previous study showing that barrier opening was at its optimum forty eight hours after suppression of claudin-5 transcripts *in vivo* (46). Barrier-modulation and administration of an identical dose of 17-AAG was repeated once more one week later. On the fifth week following the initial rAAV injection, eyes were extracted from all animals for histopathological examination. Interestingly, retinal sections demonstrated that systemic delivery of 17-AAG coupled with iBRB modulation significantly protected the ONL from degeneration, as compared to animals that did not receive claudin-5 siRNAs (Fig. 7A). In addition, the average positively transduced ONL area per unit length was compared between these animals, and eyes from animals treated with 17-AAG plus barrier modulation displayed a significantly larger ONL area per unit length (27.29 ± 1.59 μm) than animals without barrier modulation (18.91 ± 0.86 μm) ($P < 0.0001$; n=5) (Fig. 7B). These data provide evidence that barrier modulation allows 17-AAG to pass through the iBRB and that it reaches a concentration high enough to elicit a therapeutic effect in photoreceptor cells.

Discussion

To date, protein misfolding and aggregation has been implicated in a growing number of human disorders including both neurodegenerative and retinal conditions (48, 49). Since many of these disorders are caused by abnormal structural rearrangements within a protein that transform it into pathological

species, the treatment of such disorders is based on approaches that prevent the formation of the pathological conformation either by suppressing the transcript prior to mutant protein translation using RNAi (2, 3), or possibly by the use of β-sheet breakers to disrupt the β-sheet conformation adopted by abnormal protein structure (50). Pharmacological Hsp90 inhibitors (GA and derivatives) have also been considered to be neuroprotective agents in their ability to induce heat shock response via intervention of HSF-1, and have been shown to be effective in suppressing protein aggregation in cellular and animal models of Huntington's disease (HD), Parkinson's disease (PD), stroke and adRP (27, 39, 51, 52, 53). In the current study, we explored the therapeutic benefits of pharmacological induction of multiple molecular chaperones by HSF-1 activating compounds for the treatment of RP10. Results from a previous study have shown that one of the missense mutations responsible for the RP10 form of adRP, Arg224Pro, identified in a Spanish family, renders IMPDH1 prone to aggregation (9, 15). Here, we provide further evidence to support this finding by showing that mutant IMPDH1 bearing the Arg224Pro mutation is prone to aggregation *in vitro* and *in vivo*. First, soft-ware assisted prediction algorithm showed that the amino acid position of the Arg224Pro missense mutation was localised in an aggregation-prone protein segment on IMPDH1, and that this particular mutation also substantially increased the folding free energy of IMPDH1 as compared to another common IMPDH1 missense mutation (Asp226Asn) (10). (In the course of folding, protein undergoes dynamic conformational changes before reaching the most stable and functional state. Interactions between *bona fide* amino acids are more stable than those between non-native ones, thus correctly folded protein has the lowest energy structure possible) (54). In view of these predictions, the Arg224Pro mutation may elicit a destabilising effect causing significant perturbation to the proper folding of

IMPDH1 protein structure, and leading to the formation of insoluble protein aggregates with ensuing induction of significant cell death over time in a dominant negative fashion similar to that observed in the class II P23H mutant of rhodopsin. In contrast, the Asp226Asn mutation has been shown to disrupt the interaction of IMPDH1 with polyribosomes containing rhodopsin mRNA, suggesting that the pathological mechanism for this particular mutation maybe the result of perturbation of rhodopsin expression that can trigger apoptosis in photoreceptor cells (55). It is not uncommon for different mutations within a given gene to elicit a diverse range of pathological behavior. For example, adRP linked mutations identified in the rhodopsin gene can be classified into six different types, with each showing a different biochemical or cellular defect ranging from improper trafficking or folding of the protein (11). Furthermore, two lines of evidence have indicated that the accumulation of insoluble mutant IMPDH1 protein aggregates, but not WT IMPDH1, is linked to disease progression in the RP10 mouse model. First, we showed in our previous report that animals sub-retinally inoculated with AAV expressing human mutant IMPDH1 (Arg224Pro) via the rhodopsin promoter displayed significant perturbation of both ONL structure and visual function (3). In stark contrast, animals sub-retinally inoculated with the same concentration of AAV expressing WT IMPDH1 did not display any detrimental effects in the retina. Secondly, *in vitro* analysis carried out in the present study also showed that over-expression of WT IMDPH1 in mammalian cells did not elicit a build-up of insoluble protein aggregates in the pellet fraction, nor induce cell death at a level comparable to that of mutant IMPDH1. Therefore these observations support the hypothesis that the pathological effect is derived from the mutant, but not the WT form of IMPDH1. We subsequently showed that the pharmacological Hsp90 inhibitor, 17-AAG, was

able to efficiently induce a heat shock response, and reduce both the formation of mutant IMPDH1 aggregates and cell death in mammalian cells. Furthermore, intra-vitreal injection of 17-AAG was able to protect photoreceptor cells from degeneration in the RP10 mouse model through the reduction of mutant IMPDH1 protein aggregates by augmenting stress-induced heat shock protein expression. It is speculated that the therapeutic effect observed here is likely to be a direct consequence of the induction of heat shock proteins by Hsp90 inhibition, which enhances the association of chaperones with mutant IMPDH1 protein aggregates that subsequently favour or promote degradation of mutant aggregates via the proteasome system as previously been shown in the P23H mutant rhodopsin and poly-glutamine induced disease models (27, 29, 39, 56). Owing to the fact that the focus of this study is on the therapeutic effects derived from Hsp90 inhibition, additional studies will be required to decipher the sequence of events involved in this process. Here, we also provide evidence that protection of photoreceptor cells was achieved in the RP10 mouse model by systemic delivery of 17-AAG in conjunction with reversible iBRB modulation. 98% of systemically-deliverable low molecular weight drugs do not cross the BBB or iBRB. In our laboratory, a barrier-modulation technique has been well-established whereby systemic administration of siRNA targeting a tight junction protein, claudin-5, renders the iBRB passively permeable to small compounds of up to approximately 1 kDa for periods of 24-36 hours post-RNAi administration (46). In particular, no significant induction of neuronal or retinal edema, and negative impact on visual function were observed with this technique. In previous studies, 17-AAG, despite having a molecular weight of 585.7, has been shown to be BBB permeable, unlike the original benzoquinone ansamycin antibiotic, GA, which is unable to cross the BBB (37, 38). However high concentrations of inhibitors were needed to achieve

an effect, for example, Dickey and colleagues reported that intra-peritoneal administration of the Hsp90 inhibitor, EC102, at a concentration of 200mg/kg, crossed the BBB to elicit a heat shock response in murine brain tissues (45). In another study, oral administration of another Hsp90 inhibitor, 17-dimethylamino-ethylamino-17-demethoxygeldanamycin (17-DMAG), was shown to traverse the BBB to abrogate a mutant androgen receptor in a transgenic mouse model of spinal and bulbar muscular atrophy (SBMA) (57). However, one common trend observed in these animal studies, in addition to the high doses required, was that repeated administration of HSP90 inhibitors over a short period of time was required to achieve therapeutic effects. For example, Waza and colleagues reported that administration of 17-AAG (25 mg/kg) three times a week was required to ablate mutant protein in the transgenic mouse model of SBMA (38). In comparison to these studies, the significance of incorporating a barrier modulating element into our delivery strategy has enabled systemic delivery of moderately lower doses of 17-AAG (30 mg/kg), and decreased administration frequency (once a week over two week period) to achieve therapeutic effects in the RP10 mouse model, as well as negating the surgical complication associated with multiple intrusive ocular delivery methods.

In conclusion, we provide proof of principle that 17-AAG treatment successfully prevents photoreceptor degeneration in the RP10 mouse model. In addition, incorporation of barrier modulation into the delivery system allows for lower doses of 17-AAG to be delivered at reduced frequency to the inner retina to elicit a therapeutic effect. The observations that AAV-mediated expression of mutant IMPDH1 in the murine retina cause a build-up of insoluble mutant protein aggregates and induces rapid photoreceptor degeneration have indicated a direct link between accumulations of protein aggregate to disease progression. Although

the exact underlying mechanism is not yet known, it would be important to establish how protein aggregation levels correlate with photoreceptor cell death in the murine retina. However, the rapidly dying photoreceptor cells following AAV transduction in our current RP10 mouse model may pose a problem in monitoring disease progression and aggregate formation. To overcome this, we are extending a previous, unpublished study which indicated that lowering the initial viral load used to induce the RP10 mouse model, generates a slower rate of retinal degeneration. Specifically, we are designing "dose escalation and de-escalation" studies in which we induce RP10 phenotypes of increasing or decreasing severity into different cohorts of mice by administering higher/lower titres of viral particles. We will then be in a better position to correlate mutant aggregate load with photoreceptor degeneration. In addition, it may be possible to construct an AAV vector expressing mutant IMPDH1 using a tetracycline-inducible promoter to allow for controlled expression of mutant protein over designated time periods to study the relationship between aggregation level and disease progression in the retina. To date, modulation of the heat shock response has gained much attention as a potential therapeutic modality in human conformational diseases, and 17-AAG is currently being used in many clinical trials as anti-tumor agent showing low toxicity in human patients (58, 59). Although the pharmacokinetic and pharmacodynamic properties of 17-AAG have been well-characterised in previous clinical trials for cancer treatment (58), it is also important to establish the efficacy as well as the relationship between Hsp90 inhibition and protein aggregation in the murine retina. Further studies set out to characterise the rate of decrease of mutant protein aggregate following 17-AAG administration over an extensive period of time will be of significant value to future retinal therapies associated with protein aggregation. Novel Hsp90 inhibitors that exhibit improved

bioavailability and pharmacokinetics are also being investigated as anti-tumor agents in clinical trials (60-62). For example, 17-DMAG, which is a water-soluble geldanamycin analogue, has shown greater solubility, bioavailability and Hsp70 inducibility than 17-AAG (35, 63). Therefore, the safety of 17-AAG in clinical trials to date augurs well for the development of future therapies for adRP associated with IMPDH1, rhodopsin or RDS-peripherin mutations by inhibition of Hsp90 through systemic delivery of low molecular weight drugs.

Materials and Methods

Construction of WT and mutant IMPDH1 expression plasmids

The generation of both WT and mutant IMPDH1 vectors bearing the Arg224Pro and Asp226Asn mutations has previously been described by Aherne et al (15). In brief, The 1.5 kb WT human cDNA insert (spanning from exon 1 to exon 14) was cloned in to the *XhoI* site of the pcDNA3.1(+) vector (Invitrogen) to produce pWTIMPDH1. The single point mutations Arg224Pro (CGC → CCC) and Asp226Asn (GAC → AAC) were introduced into the WT human IMPDH1 cDNA by site-directed mutagenesis, and cloned into the *XhoI* site of pcDNA3.1(+) to generate pMutIMPDH1(224) and pMutIMPDH1(226), respectively. Reporter plasmids were generated by excising the EGFP gene (630 bp) from pEGFP-N1 (Clontech, BD Biosciences, Inc), and inserted between the *HindIII* and *NotI* sites of pWTIMPDH1and pMutIMPDH1(224), which was upstream of the IMPDH1 insert, creating pWTIMPDH1.EGFP and pMutIMPDH1(224).EGFP.

Cell culture and cell transfection

HeLa cells (ATCC Number: CCL-2) were cultured in Dulbecco's modified Eagle medium (DMEM, Gibco-BRL) supplemented with 10% fetal calf serum (FCS),

1% L-glutamine (2mM), sodium pyruvate (2mM) and 1% streptomucin/penicillin, in a 5% CO_2 incubator at 37°C. Cultured cells were passaged regularly with trypsin-EDTA (Gibco-BRL) to maintain exponential growth. 24 hours prior to transfection either 1 x 10^5 cells were plated out in each well of a 24-well plate or 5 x 10^5 cells were plated out in each well of a 6-well plate. Quantities of plasmid ranging from 1 µg to 2 ng were transfected into 5 x 10^5 cells using Lipofectamine 2000 as outlined by the manufacturers (Invitrogen).

Total RNA isolation and quantitative Real-Time RT-PCR analysis

Total RNA was extracted from transfected cells using TRIzol reagent (MRC) according to manufacturer's protocol. RNA was quantified using a Quantitect SYBR Green Kit as outlined by the manufacturer (Qiagen-Xeragon) under the following reaction conditions: 50°C for 20 min; 95°C for 15 min; 35 cycles of 95°C for 15 s, 57°C for 20 s, 72°C for 8 s; 95-65°C for 10 s and 40°C for 30s. Complementary primers (Sigma-Genosys, Cambridge, UK) for amplifying DNA sequences: Human Hsp90 (NM_001017963.2) →forward 5'tctggcatctgatggtgtct 3' and reverse 5'tctgtctgaaggccagtgac 3'; Human Hsp70 (NM_153201.1) → forward 5' tgtcctggttggtggttcta 3' and reverse 5'tgtctccagacaagatggct 3'; Human Hsp40 → forward 5'tctgtgtctttgggcttctg 3' and reverse 5'gagcaagacatgggagacaa 3'; Human (XM004814) and mouse (EF095208) β-actin → 5' tcacccacactgtgcccatctacga 3' and reverse 5' cagcggaaccgctcattgccaatgg 3'. The levels of heat shock protein transcripts were standardised per unit β-actin expression.

Therapeutic agents

17-Allylamino-17-demethoxygeldanamycin (17-AAG) was supplied by A.G. Scientific, Inc. and reconstituted in 0.5 ml dimethyl sulphoxide (DMSO) Hybri-Max® (Sigma) to give 10 mg/ml final stock solution.

Cleaved caspase-3 immunostaining

HeLa cells were plated at 1×10^5 cells/ml in a 24-well plate containing poly-L-lysine coated coverslips one day prior to transfection. Cells were separately transfected with 1 µg/µl pcDNA.EGFP, pWTIMPDH1.EGFP and pMut224IMPDH1.EGFP respectively using Lipofectamine 2000 (Invitrogen) according to manufacturer's protocol. 24 hours post-transfection, poly-L-lysine slides were washed in phosphate buffer saline (PBS), and fixed in 4% paraformaldehyde (pH 7.4) for 15 min at room temperature. After extensive washing in PBS, slides were incubated with cleaved caspase-3 (Asp175) antibody (1:300) (Cell Signaling Technology) overnight at 4°C, and then counterstained with Cy3-conjugated goat polyclonal to rabbit IgG (1:300) at 37°C for 2 hours. Slides were then washed and stained with 4'.6-diamindino-2-phenylindole (DAPI) (1:5000). Transfected cells were visualised under a fluorescent microscope (Zeiss, Axioplan 2). EGFP and Cy-3 positive cells in six different viewing fields (20X) from duplicate coverslips were scored blindly in two independent experiments. Transfection efficiency was calculated by standardizing the number of EGFP positive cells against the total number of cells stained by DAPI in a given field. Percentage cell death was quantified by standardising positive cleaved caspase-3 cells against EGFP-positive transfected cells. Data shown represent averages from experiments carried out twice in duplicates under the same conditions.

Western blot analysis, cellular fractionation assay and immunoprecipitation

Protein extracts were isolated from cultured cells and total retinal tissues by passing through 21-gauge syringes in protein lysis buffer containing 62.5 mM Tris, 2% SDS, 10mM Dithioreitol and 10 µl protease inhibitor cocktail/ 100 ml (Sigma Aldrich, Ireland).The homogenate was centrifuged at 8,000 rpm (Microlite 851, Thermo Electron Corporation) at 4 ^{o}C for 20 min and the supernatant was stored at -20 ^{o}C. Protein concentration was determined by BCA Protein assay kit (Pierce) with bovine serum albumin (BSA) at 2 mg/ml as standards on 96-well plates according to manufacturer's protocol. 30 µg of total protein was loaded in each lane. Protein samples were separated by electrophoresis on 10% SDS-polyacrylamide gels under reducing conditions, and transferred to nitrocellulose membranes. Primary antibodies used were as follows: anti-N-IMPDH1 (1:7000); rabbit polyclonal to cleaved caspase-3 (Asp175) (Cell Signaling Technology) (1:1000) and rabbit polyclonal to Hsp40, Hsp70 and Hsp90 (Cell Signaling Technology) (1:1000). Blots were washed with TBS and incubated with Horse Radish Peroxidase-conjugated polyclonal rabbit IgG secondary antibody (Abcam) (1:2500). Each blot was stripped with Restore Western Blot Stripping Buffer (Pierce, IL, USA) and probed with rabbit polyclonal to β-actin (Abcam) (1:2000) as loading controls. For insoluble pellet fractions, an identical gel stained with PageBlue protein staining solution (Fermentas Life Sciences) was used as loading controls. The blots were developed using enhanced chemiluminescent kit (Pierce Chemical Co.) and exposed to Fugi X-ray films in a dark-room facility.

Cellular Fractionation Assay

A protein isolation protocol for extraction of cell fractions was previously described in Aherne et al (15). In brief, cell pellets from cultured cells or total

retinal tissues were resuspended in 1 ml Buffer A containing 10mM HEPES pH

7.9, 1.5 mM $MgCl_2$, 10 mM KCl, 0.5 mM DTT, 0.5 mM PMSF, 0.25 mM

benzamidine. Cells were incubated on ice for 10 min and re-pelleted by

centrifugation at 2,000 rpm at 4°C for 10 min. Cells were resuspended in 300 µl

Buffer A, and 100 µl sample was removed from each prep for whole cell protein

analysis. NaCl was added to this aliquot to a concentration of 1 M to lyse cell

membranes. Nonidet P-40 was added to the remaining 200 µl cell suspension to a

concentration of 0.2 % and incubated on ice for 10 min. The cell suspension was

centrifuged at 3,500 rpm for 10 min at 4°C. The supernatant which contains the

soluble cytosolic proteins was removed, and the pellet containing the nuclei and

insoluble fractions was resuspended in 200 µl Buffer B (5 mM HEPES pH 7.9,

1.5 mM $MgCl_2$, 0.2 mM EDTA, 0.5 mM PMSF, 0.25 mM bezamidine) and NaCl

was added to a final concentration of 1 M. The cell suspension was then incubated

on ice for 45 min and viscosity was reduced by passing through a 25-gauge

needle. The suspension was then centrifuged at 13,000 rpm for 40 min at 4 °C.

The supernatant containing soluble nuclear proteins was preserved, and the final

pellet was resuspended in 100 µl 0.1 % SDS to denature and solublise remaining

proteins.

Immunoprecipitation

Forty-eight hours post-transfection, HeLa cells were lysed with NP40-lysis buffer

(150 mM NaCl/ 1% NP-40/ 1:10 protease inhibitor cocktail (Sigma-Aldrich)/

50mM Tris pH8) and 400 µg of total protein in 100 µl was incubated for 30 min at

4°C. Hsp90 and Hsp70 was immunoprecipitated using 1:50 dilution of rabbit

polyclonal Hsp90 and Hsp70 antibodies (Cell Signaling Technology). The

complex was recovered by incubation with 20 µl protein A-Agarose beads

(Sigma) overnight at 4°C with constant rotation. Beads were collected by

centrifugation at 2,000 rpm for 30 sec and washed in NP40-lysis buffer three times and resuspended in 50 µl of 1X electrophoresis sample buffer, heated for 5 min at 95 °C, and centrifuged to pellet the beads. Supernatants were then used to probe for IMPDH1 by Western blot analysis.

Generation of recombinant adeno-associated viral (rAAV) vectors

rAAVs were prepared as previously described in Tam et al. (3). In brief, the CMV promoter in pAAV-IRES-EGFP was replaced with 1.7 kb mouse rhodopsin promoter excised from the 17.1 kb mouse rhodopsin genomic clone to create pAAV-Rho-IRES-hrGFP (64), and human mutant IMPDH1 cDNAs bearing the Arg224Pro mutation was subcloned into this vector to create pAAVMut224IMPDH1.hrGFP. All batches of rAAVs were generated commercially by Vector Biolabs (PA, USA).

Animals and injections

The use of animals and injections carried out in this study was in accordance with the European Communities Regulations 2002 and 2005 and the Association for Research in Vision and Ophthalmology statement for the use of Animals in Ophthalmic and Vision Research, and were approved by the institutional Ethics Committee. C57/BJ6 (Harlan, UK) mice were bred and maintained in a 12 hour light-dark cycle.

Sub-retinal injections

Adult mice were anesthetized by intra-peritoneal (i.p) injection of domitor and ketamine (10 and 750 µg/10 g body weight, respectively). Pupils were dilated with 1% cyclopentolate and 2.5% phenylephrine, and under local analgesia (Amethocaine), a small puncture was administered in the sclera. Under

microscopic control, a 34-gauge blunt-ended micro-needle attached to a 10 µl

syringe (Hamilton, Bonaduz, Switzerland) was inserted through the puncture, and

a single 3 µl of 5 x 10^{11} to 1 x 10^{12} vp/ml rAAV vectors in PBS was administered

to the sub-retinal space, and a retinal detachment was induced. Following surgery,

a reversing agent (100 µg/ 10 g body weight, Atipamezole Hydrochloride) was

delivered by intraperitoneal injection. Body temperature was maintained using a

homeothermic heating device.

Intra-vitreal injections

After anesthesia and dilation of the pupil, the anterior chamber was entered via the

limbus with a 28-gauge needle to decompress the eye. Under microscopic control,

a 32-gauge (blunt) needle was passed through a sclera incision (behind the

limbus), into the vitreous cavity. A Hamilton syringe was used to dispense 3 µl of

therapeutic agent.

Preparation of *in vivo-jetPEI*/siRNA complexes: siRNA-mediated inner-blood retina barrier modulation

20 µg of claudin-5 siRNA (20 µl) was added to 100 µl of a 10 % glucose solution.

The volume was adjusted to 200 µl using RNAse/DNAse free water. The solution

was mixed and briefly centrifuged. In a separate tube, 6.4 µl of *in vivo-JetPEI*

(Polyplus Transfection) was added to100 µl of a 10 % glucose solution. The

volume was adjusted to 200 µl using RNAse/DNAse free water, mixed and briefly

centrifuged. The 200 µl of *in vivo-JetPEI* solution was then added to the siRNA

solution (ensuring solution were mixed in this order not the other way around).

Solutions were vortexed and briefly centrifuged. The complexes were incubated

for 15 min at room temperature and administered into mice by rapid high-

pressure, high-volume tail vein injections as previously described (46, 65). Forty

eight hours post-injection of siRNA, mice were injected with a solution of 17-AAG at a dose of 30 mg/kg intra-peritoneally. This procedure was repeated twice over the course of 14 days.

Immunohistochemistry and histopathology

Whole eyes were extracted from injected mice and immediately fixed in 4% paraformaldehyde (pH 7.4) for 4 hours at 4°C on a rotating device. Eyes were then washed in PBS for 1 hour and sequentially submerged in 10%, 20% and 30% sucrose. Whole eyes were then suspended in specimen blocks with OCT solution (Tissue Tek) and snap frozen with liquid nitrogen. Frozen eyes were sectioned using a cryo-sectioner (Leica CM 1900) to 12 μm thickness. Sections were collected on Polysine® slides (Menzel-Glazer). To detect hrGFP, retinal sections were blocked for 20 min at room temperature in PBS containing 5% goat serum, and immunostained with Vitality® full length hrGFP polyclonal antibody (Stratagene) (1:100) overnight at 4°C in a humidity chamber. Sectioned retinas were then washed three times in PBS and incubated with Cy-2 labeled anti-rabbit IgG antibody (Abcam) for 1 hr at 37°C in a humidity chamber. Following incubation, sections were washed with PBS and mounted with aqua-polymount (Polyscience) after nuclei-counterstaining with DAPI (1:5000). Retinal sections were visualized using fluorescent microscope (Zeiss Axioplan 2, Oberkochen, Germany) and confocal microscope (Olympus FluoView TM FV 1000). To evaluate quantitatively the area per unit length (μm) of positively transduced ONL, retinal sections were viewed under a fluorescent microscope (Zeiss, Axioplan 2). hrGFP positive ONL areas from twelve independent sections from each eye were measured using analytical software tools (Analysis B, Zeiss), and the average area per unit length for each treated animal was grouped, and the

average positively transduced ONL area per unit length was compared to control eyes.

Statistical Analysis

For all experiments presented in this study; mean values, standard error of the mean (SEM) and paired Student's t-tests were calculated using GraphPad Prism version 5.0. Differences were considered statistically significant at P values $\leq$ 0.05.

References

1. Hartong, D.T., Berson, E.L., and Dryja, T.P. (2006) Retinitis pigmentosa. *Lancet*., **368**, 1795-1809.

2. O'Reilly, M., Palfi, A., Chadderton, N., Millington-Ward, S., Ader, M., Cronin, T., Tuohy, T., Auricchio, A., Hildinger, M., Tivnan, A., et al (2007) RNA interference-mediated suppression and replacement of human rhodopsin *in vivo*. *Am. J. Hum. Genet*., **81**, 127-35.

3. Tam, L.C., Kiang, A.S., Kennan, A., Kenna, P.F., Chadderton, N., Ader, M., Palfi, A., Aherne, A., Ayuso, C., Campbell, M., Reynolds, A., et al (2008) Therapeutic benefit derived from RNAi-mediated ablation of IMPDH1 transcripts in a murine model of autosomal dominant retinitis pigmentosa (RP10). *Hum. Mol. Genet*., **17**, 2084-2100.

4. Bainbridge, J.W., Smith, A.J., Barker, S.S., Robbie, S., Henderson, R., Balaggan, K., Viswanathan, A., Holder, G.E., Stockman, A., Tyler, N., et al (2008) Effect of gene therapy on visual function in Leber's congenital amaurosis. *N. Engl. J. Med*., **358**, 2231-2239.

5. Cideciyan, A.V., Hauswirth, W.W., Aleman, T.S., Kaushal, S., Schwartz, S.B., Boye, S.L., Windsor, E.A., Conlon, T.J., Sumaroka, A., Pang, J.J., et al (2009) Human RPE65 gene therapy for Leber congenital amaurosis: persistence of early visual improvements and safety at 1 year. *Hum Gene Ther.,* **20**, 999-1004.

6. Maguire, A.M., High, K.A., Auricchio, A., Wright, J.F., Pierce, E.A., Testa, F., Mingozzi, F., Bennicelli, J.L., Ying, G.S., Rossi, S., et al (2009) Age-dependent effects of RPE65 gene therapy for Leber's congenital amaurosis: a phase 1 dose-escalation trial. *Lancet.,* **374**, 1597-1605.

7. Dryja, T.P., McGee, T.L., Reichel, E., Hahn, L.B., Cowley, G.S., Yandell, D.W., Sandberg, M.A., and Berson, E.L. (1990) A point mutation of the rhodopsin gene in one form of retinitis pigmentosa. *Nature.,* **343**, 364-366.

8. Farrar, G.J., Kenna, P., Jordan, S.A., Kumar-Singh, R., Humphries, M.M., Sharp, E.M., Sheils, D.M. and Humphries, P. (1991) A three-base-pair deletion in the peripherin-RDS gene in one form of retinitis pigmentosa. Nature. *354*, 478-80.

9. Kennan, A., Aherne, A,, Palfi, A., Humphries, M.M., McKee, A., Stitt, A., Simpson, D.A., Demtroder, K., Orntoft, T., Ayuso, C., Kenna P.F., Farrar, G.J., and Humphries, P. (2002) Identification of an IMPDH1 mutation in autosomal dominant retinitis pigmentosa (RP10) revealed following comparative microarray analysis of transcripts derived from retinas of wild-type and Rho(-/-) mice. *Hum. Mol. Genet.,* **11**, 547-557.

10. Bowne, S.J., Sullivan, L.S., Blanton, S.H., Cepko, C.L., Blackshaw, S., Birch, D.G., Hughbanks-Wheaton, D., Heckenlively, J.R. and Daiger, S.P. (2002) Mutations in the inosine monophosphate dehydrogenase 1 gene (IMPDH1) cause the RP10 form of autosomal dominant retinitis pigmentosa. *Hum. Mol. Genet.,* **11**, 559-568.

11. Mendes, H.F., van der Spuy, J., Chapple, J.P., and Cheetham, M.E. (2005) Mechanisms of cell death in rhodopsin retinitis pigmentosa: implications for therapy. *Trends Mol. Med.,* **11**,177-185.

12. Illing, M.E., Rajan, R.S., Bence, N.F., and Kopito, R.R. (2002) A rhodopsin mutant linked to autosomal dominant RP is prone to aggregate and interacts with the ubiquitin proteasome system. *J. Biol. Chem.* **277**, 34150 –34160.

13. Saliba, R.S., Munro, P.M., Luthert, P.J., and Cheetham, M.E. (2002) The cellular fate of mutant rhodopsin: quality control, degradation and aggresome formation. *J. Cell Sci*., **115**, 2907-2918.

14. Conley, S.M., Stricker, H.M., and Naash, M.I. (2010) Biochemical analysis of phenotypic diversity associated with mutations in codon 244 of the retinal degeneration slow gene. *Biochemistry*., **49**, 905-911.

15. Aherne, A., Kennan, A., Kenna, P.F., McNally, N., Lloyd, D.G., Alberts, I.L., Kiang, A.S., Humphries, M.M., Ayuso, C., Engel, P.C., et al (2004) On the molecular pathology of neurodegeneration in IMPDH1-based retinitis pigmentosa. *Hum. Mol. Genet*., **13**, 641-650.

16. Olsson, J.E., Gordon, J.W., Pawlyk, B.S., Roof, D., Hayes, A., Molday, R.S., Mukai, S., Cowley, G.S., Berson, E.L., and Dryja, T.P. (1992) Transgenic mice with a rhodopsin mutation (Pro23His): a mouse model of autosomal dominant retinitis pigmentosa. *Neuron*., **9**, 815-830.

17. Kosmaoglou, M., Schwarz, N., Bett, J.S., and Cheetham, M.E. (2008) Molecular chaperones and photoreceptor function. *Prog. Retin. Eye. Res*., **27**, 434-449.

18. Macario, A.J., Grippo, T.M., and de Macario, E.C. (2005) Genetic disorders involving molecular-chaperone genes: A perspective. *Genet. Med*., **7**, 3-12.

19. Hayashi, M., Imanaka-Yoshida, T., Wood, M., Fearns, C., Tatake, R.J., and Lee, J.D. (2006) A crucial role of mitochondria Hsp40 in precenting dilated cardiomyopathy. *Nat. Med*. **12**, 128-132.

20. Stock, A.D., Spallone, P.A., Dennis, T.R., Netski, D., Morris, C.A., Mervis, C.B., and Hobart, H.H. (2003) Heat shock protein 27 gene:

chromosomal and molecular location and relationship to Williams syndrome. *Am. J. Med. Genet. A.*, **120A**, 320-325.

21. Hidalgo-de-Quintana, J., Evans, R.J., Cheetham, M.E., and van der Spuy, J. (2008) The Leber congenital amaurosis protein AIPL1 functions as part of a chaperone heterocomplex. *Invest. Ophthalmol. Vis. Sci.*, **49**, 2878-2887.

22. Parsell, D.A., and Lindquist, S. (1993) The function of heat-shock proteins in stress tolerance: degradation and reactivation of damaged proteins. *Annu. Rev. Genet.*, **27**, 437-96.

23. Pratt, W.B., and Toft, D.O. (2003) Regulation of signaling protein function and trafficking by the hsp90/hsp70-based chaperone machinery. *Exp. Biol. Med.*, **228**, 111-133.

24. Mayer, M.P., and Bukau, B. (2005) Hsp70 chaperones: cellular functions and molecular mechanism. *Cell Mol. Life Sci.*, **62**, 670-684.

25. Young, J.C., Agashe, V.R., Seigers, K., and Hartl, F.U. (2004) Pathways of chaperone-mediated protein folding in the cytosol. *Nat. Rev. Mol. Cell. Biol.*, **5**, 781-791.

26. Hirayama, S., Yamazaki, Y., Kitamura, A., Oda, Y., Morito, D., Okawa, K., Kimura, H., Cyr, D.M., Kubota, H., and Nagata, K. (2008) MKKS is a centrosome-shuttling protein degraded by disease-causing mutations via CHIP-mediated ubiquitination. *Mol. Biol. Cell.*, **19**, 899-911.

27. Sittler, A., Lurz, R., Lueder, G., Priller, J., Lehrach, H., Hayer-Hartl, M.K., Hartl, F.U., and Wanker, E.E. (2001) Geldanamycin activates a heat shock response and inhibits huntingtin aggregation in a cell culture model of Huntington's disease. Hum. Mol. Genet., **10**, 1307-1315.

28. Warrick, J.M., Chan, H.Y., Gray-Board, G.L., Chai, Y., Paulson, H.L., and Bonini, N.M. (1999) Suppression of polyglutamine-mediated neurodegeneration in Drosophila by the molecular chaperone HSP70. *Nat. Genet.*, **23**, 425-428.

29. Chan, H.Y., Warrick, J.M., Gray-Board, G.L., Paulson, H.L., and Bonini, N.M. (2000) Mechanisms of chaperone suppression of polyglutamine disease: selectivity, synergy and modulation of protein solubility in Drosophila. *Hum. Mol. Genet.*, **9**, 2811-2820.

30. Gorbatyuk, M.S., Knox, T., LaVail, M.M., Gorbatyuk, O.S., Noorwez, S.M., Hauswirth, W.W., Lin, J.H., Muzyczka, N., and Lewin, A.S. (2010) Restoration of visual function in P23H rhodopsin transgenic rats by gene delivery of BiP/Grp78. *Proc. Natl. Acad. Sci. U.S.A.*, **107**, 5961-5966.

31. Sloan, L.A., Fillmore, M.C., and Churcher, I. (2009) Small-molecule modulation of cellular chaperones to treat protein misfolding disorders. *Curr. Opin. Drug Discov. Devel.*, **12**, 666-681.

32. Harrison, P.J., Procter, A.W., Exworthy, T., Roberts, G.W., Najlerahim, A., Barton, A.J., and Pearson, R.C. (1993) Heat shock protein (hsx70) mRNA expression in human brain: effects of neurodegenerative disease and agonal state. *Neuropathol. Appl. Neurobiol.*, **19**, 10-21.

33. Fukuyo, Y., Hunt, C.R., and Horikoshi, N. (2010) Geldanamycin and its anti-cancer activities. *Cancer Lett.*, **290**, 24-35.

34. Zou, J., Guo, Y., Guettouche, T., Smith, D.F., and Voellmy, R. (1998). Repression of heat shock transcription factor HSF1 activation by HSP90 (HSP90 complex) that forms a stress-sensitive complex with HSF1. *Cell.*, **94**, 471-480.

35. Egorin, M.J., Zuhowski, E.G., Rosen, D.M., Sentz, D.L., Covey, J.M., and
    Eiseman, J.L. (2001) Plasma pharmacokinetics and tissue distribution of
    17-(allylamino)-17-demethoxygeldanamycin (NSC 330507) in CD2F1
    mice1. *Cancer Chemother. Pharmacol.*, **47**, 291-302.

36. Sausville, E.A., Tomaszewski, J.E., and Ivy, P. (2003) Clinical
    development of 17-allylamino, 17-demethoxygeldanamycin. *Curr. Cancer
    Drug Targets*, **3**, 377-383.

37. Fujikake, N., Nagai, Y., Popiel, H.A., Okamoto, Y., Yamaguchi, M., and
    Toda, T. (2008) Heat shock transcription factor 1-activating compounds
    suppress polyglutamine-induced neurodegeneration through induction of
    multiple molecular chaperones. *J. Biol. Chem.*, **283**, 26188-26189.

38. Waza, M., Adachi, H., Katsuno, M., Minamiyama, M., Sang, C., Tanaka,
    F., Inukai, A., Doyu, M., and Sobue, G. (2005) 17-AAG, an Hsp90
    inhibitor, ameliorates polyglutamine-mediated motor neuron degeneration.
    Nat. Med., **11**, 1088-1095.

39. Mendes, H.F., and Cheetham. M.E. (2008) Pharmacological manipulation
    of gain-of-function and dominant-negative mechanisms in rhodopsin
    retinitis pigmentosa. *Hum. Mol. Gen.*, **17**, 3043-3054.

40. Sharp, S., and Workman, P. (2006) Inhibitors of the HSP90 molecular
    chaperone: current status. *Adv. Cancer Res.*, **95**, 323-348.

41. Conchillo-Solé, O., de Groot, N.S., Avilés, F.X., Vendrell, J., Daura, X.,
    and Ventura, S. (2007) AGGRESCAN: a server for the prediction and
    evaluation of "hot spots" of aggregation in polypeptides. *BMC
    Bioinformatics*, **8**, 65.

42. Dehouck, Y., Grosfils, A., Folch, B., Gilis, D., Bogaerts, P., and Rooman,
    M. (2009) Fast and accurate predictions of protein stability changes upon

mutations using statistical potentials and neural networks: PoPMuSiC-2.0. *Bioinformatics*, **25**, 2537-2543.

43. Fernandes-Alnemri, T., Litwack, G., and Alnemri, E.S. (1994) CPP32, a novel human apoptotic protein with homology to Caenorhabditis elegans cell death protein Ced-3 and mammalian interleukin-1 beta-converting enzyme. *J. Biol. Chem*., **269**, 30761-30764.

44. Nicholson, D.W., Ali, A., Thornberry, N.A., Vaillancourt, J.P., Ding, C.K., Gallant, M., Gareau, Y., Griffin, P.R., Labelle, M., Lazebnik, Y.A., et al. (1995). Identification and inhibition of the ICE/CED-3 protease necessary for mammalian apoptosis. *Nature*, **376**, 37-43.

45. Dickey, C.A., Kama,l A., Lundgren, K., Klosak, N., Bailey, R.M., Dunmore, J., Ash, P., Shoraka, S., Zlatkovic, J., Eckman, C.B., et al. (2007) The high-affinity HSP90-CHIP complex recognizes and selectively degrades phosphorylated tau client proteins. *J. Clin. Invest*., **117**, 648-658.

46. Campbell, M., Nguyen, A.T., Kiang, A.S., Tam, L.C., Gobbo, O.L., Kerskens, C., Ni Dhubhghaill, S., Humphries, M.M., Farrar, G.J., Kenna, P.F., and Humphries. P. (2009) An experimental platform for systemic drug delivery to the retina. *Proc. Natl. Acad. Sci. U.S.A*., **106**, 17817-17822.

47. Campbell, M., Kiang, A.S., Kenna, P.F., Kerskens, C., Blau, C., O'Dwyer, L., Tivnan, A., Kelly, J.A., Brankin, B., Farrar, G.J., and Humphries, P. (2008) RNAi-mediated reversible opening of the blood-brain barrier. *J. Gene. Med.*, **10**, 930-947.

48. Ross, C.A., and Poirier, M.A. (2004) Protein aggregation and neurodegenerative disease. *Nat, Med*., **10**, S10-17.

49. Surguchev, A., and Surguchov, A. (2009) Conformational diseases: Looking into the eyes. *Brain Research Bulletin*, **81**, 12-24.

50. Wisniewski, T., and Sadowski, M. (2008) Preventing beta-amyloid fibrillization and deposition: beta-sheet breakers and pathological chaperone inhibitors. *BMC. Neurosci.*, **9**, S5.

51. Herbst, M., and Wanker, E.E. (2007) Small molecule inducers of heat-shock response reduce polyQ-mediated huntingtin aggregation. A possible therapeutic strategy. *Neurodegener. Dis.*, **4**, 254-260.

52. Auluck, P.K., and Bonini, N.M. (2002) Pharmacological prevention of Parkinson disease in Drosophila. *Nat. Med.*, **8**, 1185-1186.

53. Lu, A., Ran, R., Parmentier-Batteur, S., Nee, A., and Sharp, F.R. (2002) Geldanamycin induces heat shock proteins in brain and protects against focal cerebral ischemia. *J. Neurochem.*, **81**, 355-364.

54. Dobson, C.M. (2002) Getting out of shape. *Nature,* **418**, 729-730.

55. Mortimer, S.E., Xu, D., McGrew, D., Hamaguchi, N., Lim, H.C., Bowne, S.J., Daiger, S.P., and Hedstrom, L. (2008) IMP dehydrogenase type 1 associates with polyribosomes translating rhodopsin mRNA. *J. Biol. Chem.*, **283**, 36354-36360.

56. Hay, D.G., Sathasivam, K., Tobaben, S., Stahl, B., Marber, M., Mestril, R., Mahal, A., Smith, D.L., Woodman, B., and Bates, G.P. (2004) Progressive decrease in chaperone protein levels in a mouse model of Huntington's disease and induction of stress proteins as a therapeutic approach. *Hum. Mol. Genet.*, **13**, 1389-1405.

57. Tokui, K., Adachi, H., Waza, M., Katsuno, M., Minamiyama, M., Doi, H., Tanaka, K., Hamazaki, J., Murata, S., et al (2009) 17-DMAG ameliorates polyglutamine-mediated motor neuron degeneration through well-

preserved proteasome function in an SBMA model mouse. *Hum. Mol. Genet.*, **18**, 898-910.

58. Ramanathan, R.K., Trump, D.L., Eiseman, J.L., Belani, C.P., Agarwala, S.S., Zuhowski, E.G., Lan J, Potter, D.M., Ivy, S.P., Ramalingam, S., et al (2005) Phase I pharmacokinetic-pharmacodynamic study of 17-(allylamino)-17-demethoxygeldanamycin (17AAG, NSC 330507), a novel inhibitor of heat shock protein 90, in patients with refractory advanced cancers. *Clin. Cancer Res*., **11**, 3385-3391.

59. Goetz, M.P., Toft, D., Reid, J., Ames, M., Stensgard, B., Safgren, S., Adjei, A.A., Sloan, J., Atherton, P., Vasile, V., et al (2005) Phase I trial of 17-allylamino-17-demethoxygeldanamycin in patients with advanced cancer. *J. Clin. Oncol*., **23**, 1078-1087.

60. Hollingshead, M., Alley, M., Burger, A.M., Borgel, S., Pacula-Cox, C., Fiebig, H.H., and Sausville, E.A. (2005) In vivo antitumor efficacy of 17-DMAG (17-dimethylaminoethylamino-17-demethoxygeldanamycin hydrochloride), a water-soluble geldanamycin derivative. *Cancer Chemother. Pharmacol*., **56**, 115-125.

61. Shadad, F.N., and Ramanathan, R.K. (2006) 17-dimethylaminoethylamino-17-demethoxygeldanamycin in patients with advanced-stage solid tumors and lymphoma: a phase I study. *Clin. Lymphoma Myeloma*, **6**, 500-501.

62. Lancet, J.E., Gojo, I., Burton, M., Quinn, M., Tighe, S.M., Kersey, K., Zhong, Z., Albitar, M.X., Bhalla, K., Hannah, A.L., et al (2010) Phase I study of the heat shock protein 90 inhibitor alvespimycin (KOS-1022, 17-DMAG) administered intravenously twice weekly to patients with acute myeloid leukemia. *Leukemia*, **24**, 699-705.

63. Wetzler, M., Earp, J.C., Brady, M.T., Keng, M.K., and Jusko, W.J. (2007). Synergism between arsenic trioxide and heat shock protein 90 inhibitors on signal transducer and activator of transcription protein 3 activity-pharmacodynamic drug-drug interaction modeling. *Clin. Cancer Res*., **13**, 2261-2270.

64. Humphries, M.M., Rancourt, D., Farrar, G.J., Kenna, P., Hazel, M., Bush, R.A., Sieving, P.A., Sheils, D.M., McNally, N., Creighton. P., et al (1997) Retinopathy induced in mice by targeted disruption of the rhodopsin gene. *Nat. Genet*., **15**, 216-219.

65. Kiang, A.S., Palfi, A., Ader, M., Kenna, P.F., Millington-Ward, S., Clark, G., Kennan, A., O'Reilly, M., Tam, L.C., Aherne, A., et al (2005) Toward a gene therapy for dominant disease: validation of an RNA interference-based mutation-independent approach. *Mol. Ther*., **12**, 555-561.

Legends to Figures

Figure 1: Heat shock protein chaperones assisted protein folding in eukaryotic cells. (A) Heat shock protein 40 (40-kDa) attached to ribosomes (rHsp40) activate and recruit cytosolic Hsp70 to associate with newly synthesised polypeptide chains. This co-translational Hsp70 chaperoning is ATP-dependent and may be sufficient to correctly fold some polypeptides; (B) while others may be passed onto the Hsp70-Hsp90 multi-component chaperone complex for further folding with the help of a co-chaperone, Hsp-organising protein (HOP). The later stages of Hsp90-assisted client protein folding are modulated by another co-chaperone, p23, which leads to the formation of a stabilised Hsp90-client protein complex to enable proper folding. (C) In the case of proteins that exhibit significant structural instability, Hsp70 can recruit the co-chaperone CHIP (U-box ubiquiting-ligase carboxyl terminus of HSC70-interacting protein) to covalently attach polyubiquitin chain onto substrate polypeptides serving as a marker for proteolytic degradation, which eventually leads to protein degradation via the 26S proteasome. The CHIP co-chaperone is docked to Hsp70 or Hsp90 holding a misfolded protein, which then recruits an E2 enzyme to initiate ubiquitinylation. The Hsp70 regulatory co-chaperone BAG-1 (BCL-2 associated athanogene-1) then links the chaperone to proteasomes to release ubiquitylated polypeptides for degradation. (D) Adverse conditions such as destabilising mutations can cause aberrant protein to manifest which may lead to (E) clearance of mutant protein via proteasome degradation with a consequent 'loss of function' phenotype, or (F) accumulation of misfolded protein result in aggregation or the formation of insoluble proteinasceous deposits causing 'gain of function' toxicity.

Figure 2: 17-AAG mediated induction of heat shock response and preferential client protein degradation in mammalian cells. Under normal physiological conditions, inactive monomeric HSF-1 is localised in the cytosol and is associated with the Hsp90 multi-chaperone complex. Upon exposure to cellular stress or stress inducers, i.e. 17-AAG, which binds to the ATP pocket on the N-terminus of Hsp90, HSF-1 dissociates from the Hsp90 complex and is activated via trimerization and phosphorylation. Subsequently, activated HSF-1 translocates into the nucleus and binds to the heat shock element in the promoter region of Hsp70 and various molecular chaperone genes to simultaneously induce their expression. Binding of 17-AAG to Hsp90 can also disrupt the association of Hsp90 complex with client proteins, altering the Hsp90 complex from stabilising form towards proteasome-targeting form, resulting in enhanced proteasome degradation of Hsp90 client proteins.

Figure 3: Formation of insoluble protein aggregates and induction of cell death by mutant IMPDH1 in HeLa cells. (A) Cellular fractionation assay illustrating dose-dependent insoluble mutant IMPDH1 protein aggregate formation in HeLa cells. Note that mutant IMPDH1 bearing the Arg224Pro mutation accumulated in the insoluble protein fraction, giving off a strong signal at 250 and 50 ng. In contrast, no or weak IMPDH1 was detected in HeLa cells transfected with empty vector, wild type IMPDH1 and mutant IMPDH1 bearing the Asp226Asn mutation. Coomassie-Blue staining of identical gels as loading controls. M = protein marker. (B) Representative fluorescent images of cleaved caspase-3 staining in HeLa cells transfected with WT or mutant IMPDH1 EGFP fusion expression plasmids. Bar charts represent percentage positive cleaved caspase-3 staining normalised against transfection efficiency. *** $P < 0.0001$. Scale bar denotes 200 μm. Data presented here represent the mean of three independent experiments

carried out in triplicate. (C) Identification of cell blebbing (indicated by arrows) in HeLa cells transfected with mutant IMPDH1 bearing the Arg224Pro mutation. Merge = Phase contrast image overlaid with EGFP. Scale bar denotes 40 μm. (D) Hsp70 and Hsp90 co-immunoprecipitates with mutant IMPDH1: Western blot analysis in HeLa cells after immunoprecipitation with IMPDH1 antibody, with total cell lysates as positive control and isotype-matched IgG as negative control. Immunoprecipitation antibodies as loading controls.

Figure 4: Effect of 17-AAG on heat shock proteins and mutant IMPDH1 in mammalian cell cultures. (A) HeLa cells were first treated with 17-AAG, and total RNA was extracted at 6, 24, 48 and 72 hours post-treatment. The relative quantities of heat shock protein transcripts were measured by Real Time RT-PCR and normalised against endogenous β-actin expression. Error bars denote standard error of the mean (SEM). (B) Similarly, whole cell lysates were prepared from DMSO or 17-AAG treated cells 48 hours post-treatment. Western blot analysis illustrates up-regulation of Hsp90, Hsp70 and Hsp40 protein expression and bar chart denotes densitometric measurements of corresponding band intensities normalised against β-actin. $*$ $P = 0.024$. Data represent average percentage ± SEM. Error bars denote standard error of the mean. (C) Western blot analysis showing 17-AAG mediated degradation of insoluble mutant IMPDH1 protein aggregates in HeLa cells. Coomassie-blue staining of identical gels was used as loading controls for the insoluble protein pellet fraction. Bar chart illustrates densitometric measurements of percentage decrease of mutant IMPDH1 in the insoluble protein pellet fraction as compared to DMSO control. $**$ $P = 0.0011$. (D) Treatment of mutant IMPDH1 transfected HeLa cells with 17-AAG also showed a decrease in cleaved caspase-3 activation as compared to DMSO control.

Figure 5: Effect of 17-AAG on heat shock proteins and mutant IMPDH1 in WT mouse retinas. (A) Western blot analyses showing the up-regulation of Hsp90, Hsp70 and Hsp40 protein expression in WT mouse retinas 24 hours following intra-vitreal administration of 17-AAG. Bar chart represents densitometric analysis showing relative fold changes among different heat shock proteins normalised against β-actin. * $P = 0.0319$. n = 3. (B) WT mice were initially injected with AAV-mutant224 and subsequently administered with 17-AAG (0.2 μg/μl) twice over 2-week period. Insoluble protein pellet fraction shows the detection of mutant IMPDH1 in eyes treated with DMSO (2%) (lanes 3 and 4), whereas significant diminished insoluble mutant protein was observed in eyes treated with 17-AAG (lanes 5 and 6). Bar chart illustrates densitometric measurements of relative fold change between control and treated eye groups. n=4. ** $P = 0.0027$. Untreated eyes (lanes 1 and 2) acted as negative controls. Coomassie-blue staining of identical gels acted as loading controls.

Figure 6: Rescue of photoreceptor cells in the RP10 mouse model following intra-vitreal injection of 17-AAG. (A) Representative images of retinal sections illustrating the rescue of photoreceptor cells in the RP10 mouse model. OS = outer segment; ONL = outer nuclear layer; INL = inner nuclear layer; GCL = ganglion cell layer. Scale bar denotes 40 μm. All images show merge hrGFP and DAPI staining. (B) Quantitative analysis of positively transduced ONL per unit length (μm) in retinal sections of vehicle control and 17-AAG treated mice. n=4. * $P = 0.0485$. Eight ONL measurements were taken from each retina. Error bars denote standard error of the mean (SEM).

Figure 7: Systemic administration of 17-AAG coupled with barrier modulation using claudin-5 targeting siRNA protects the ONL in the RP10 mouse model. WT

mice were first sub-retinally injected with AAV-mutant224. Two weeks post

injection claudin-5 siRNA was administered using *in vivoJet-PEI* by high pressure

tail vein injection. 48-hours post-barrier modulation, 17-AAG was administered

systemically by i.p injection, and claudin-5 siRNA and 17-AAG were

administered once more a week later. (A) Retinal sections (12 μm) were

immunostained with hrGFP primary antibody and counterstained with goat

polyclonal to rabbit IgG Cy2 secondary antibody. Green=hrGFP. Blue=DAPI.

ONL = outer nuclear layer; INL = inner nuclear layer. All images show merge

hrGFP and DAPI staining. Scale bar denotes 20 µm. (B) Data represent average

positively transduced ONL area per unit length (µm) ± SEM. *** $P \leq 0.0001$.

n=5. Error bars denote standard error of the mean (SEM).

Abbreviations

AAV: Adeno-associated virus

adRP: Autosomal dominant retinitis pigmentosa

BBB: Blood brain barrier

Hsp: Heat shock protein

iBRB: Inner blood retina barrier

IMPDH1: Inosine 5'-monophosphate dehydrogenase type 1

LCA: Leber congenital amaurosis

ONL: Outer nuclear layer

RNAi: RNA interference

RP: Retinitis pigmentosa

siRNA: Small interfering RNA

WT: Wild type

17-AAG: 17-(Allylamino)-17-demethoxygeldanamycin

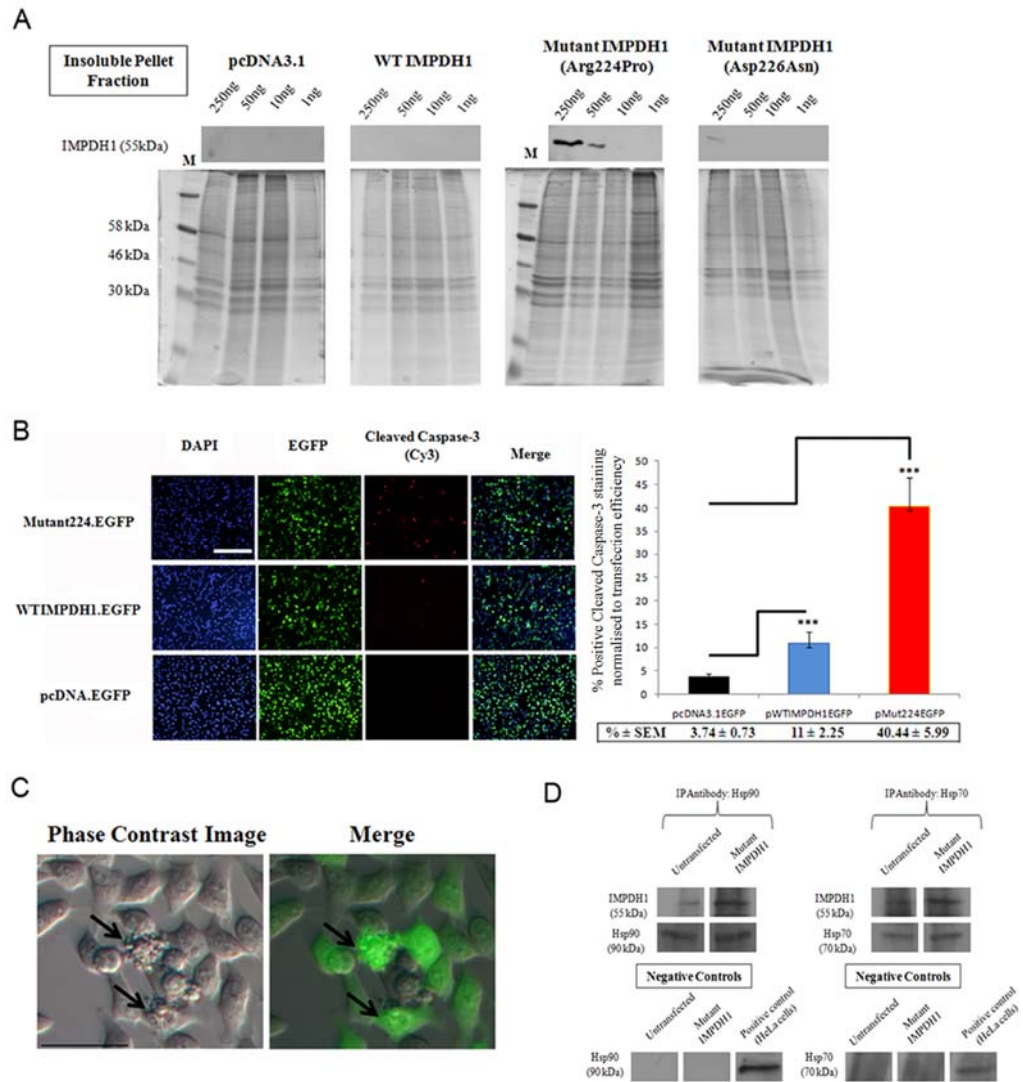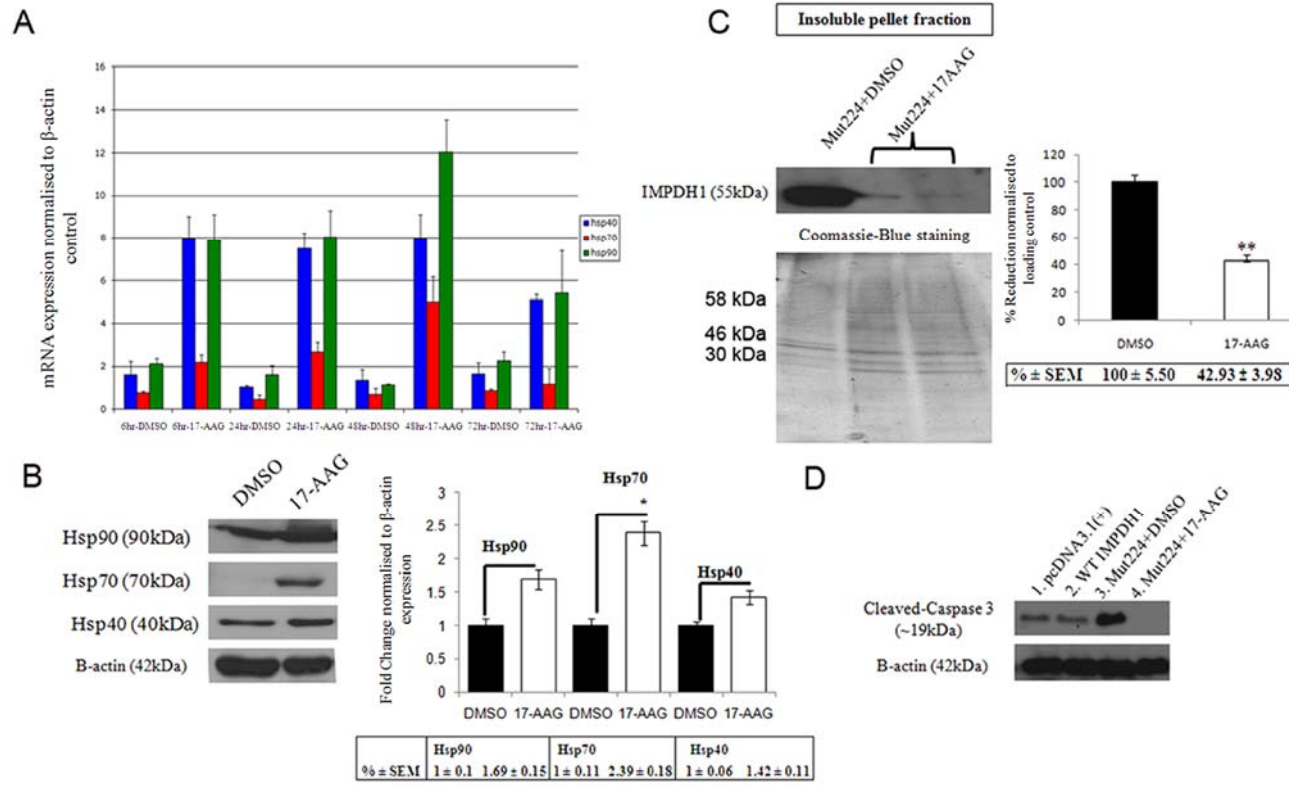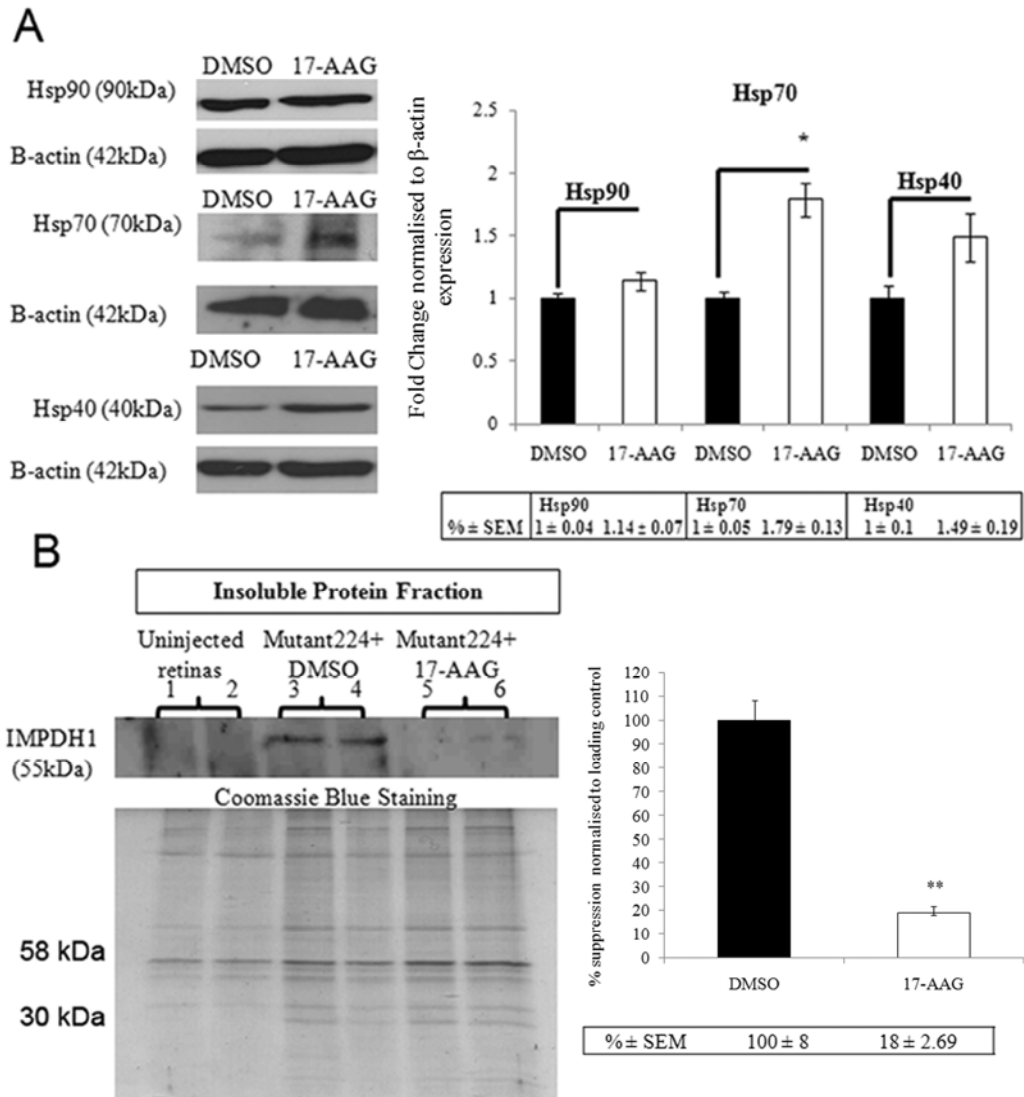17-DMAG: 17-Dimethylamino-ethylamino-17-demethoxygeldanamycin

Figure 1
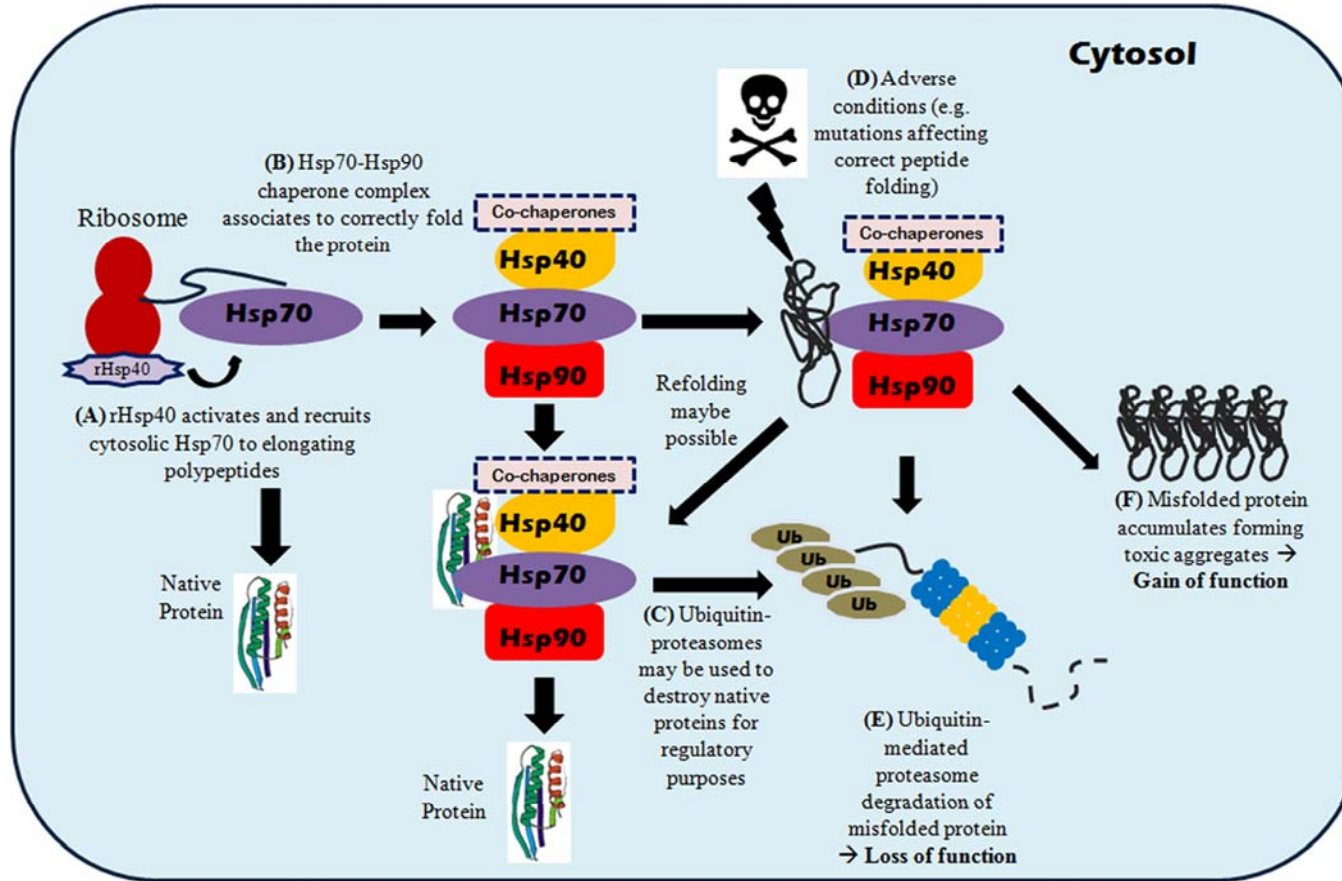
Figure 2
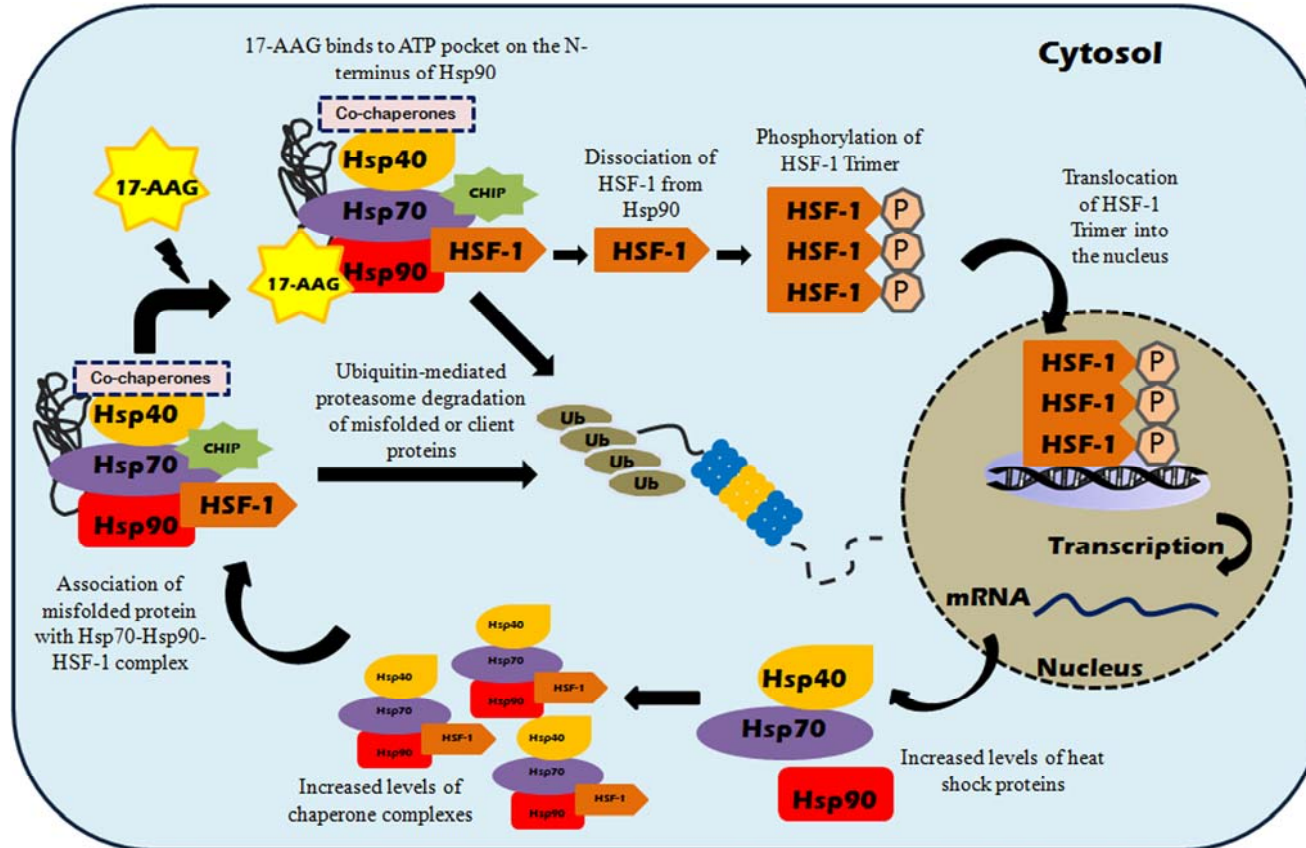
Figure 3

Figure 4

Figure 5

Figure 6

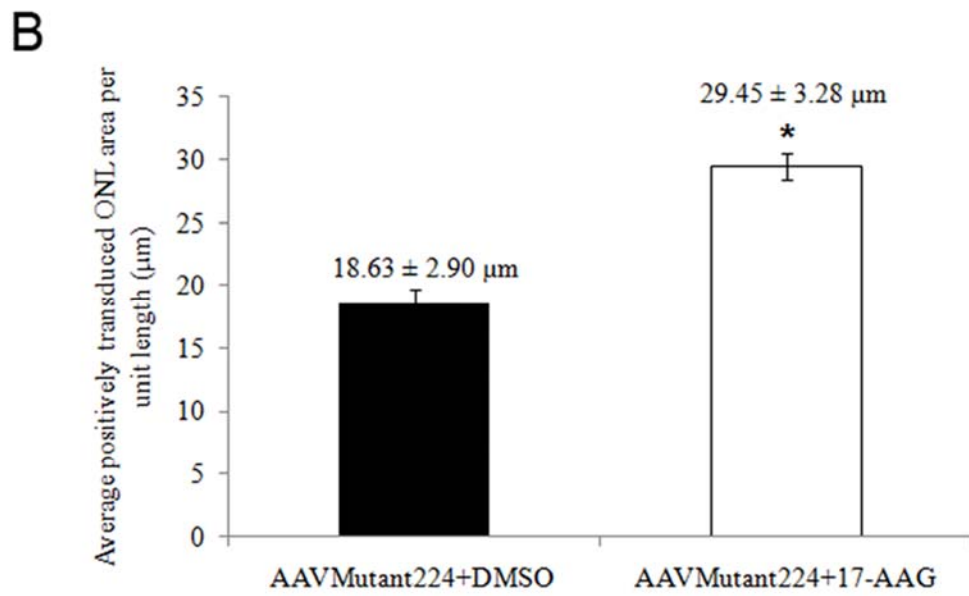Figure 7

A   Mutant 224+ siNT + 17-AAG   Mutant 224+ siClaudin-5 + 17-AAG

ONL   ONL

INL   INL

                    20um   20um

B

27.29 ± 1.59 µm

18.91 ± 0.85 µm

***

Average positively transduced
ONL area per unit length (µm)

35
30
25
20
15
10
5
0

Mutant224+siNT+17-AAG   Mutant224+siClaudin5+17-AAG